The AKARI diffuse maps

Conference or Workshop Item

SPICA Workshop, 03006 (2009)
DOI:10.1051/spica/200903006

THE AKARI DIFFUSE MAPS

M. Etxaluze[1,2], Y. Doi[3], D. Kester[4], G.J. White[1,2], E. Figueredo[5], Y. Chinone[6], M. Hattori[6], T. Nakagawa[7], C. Yamamuchi[7], H. Shibai[8,9] and The AKARI team

[1]Department of Physics & Astronomy, The Open University, UK
[2]Space Science & Technology Dep., Rutherford Appleton Laboratory, UK
[3]Department of General System Studies, Graduate School of Arts and Sciences, The University of Tokyo, Japan
[4]Netherlands Institute for Space Research SRON, Netherlands
[5]Instituto de Astronomía, Geofísica e Ciencias Atmosféricas, Universidade de São Paolo, Brazil
[6]Astronomical Institute, Tohoku University, Japan
[7]Institute of Space and Astronautical Sciences, JAXA, Japan
[8]Graduate School of Sciences, Nagoya University, Japan
[9]Graduate School of Sciences, Osaka University, Japan

Abstract

We descibe the calibration of maps of diffuse Galactic Plane emission, and present detailed observations of several complexes. We put especial atention on Cygnus X region showing its temperature and density maps.

1. Introduction

Maps of the diffuse Galactic Plane emission with AKARI provide a considerable increase in sharpness and fidelity over previously available data from the IRAS all sky survey, and cover much larger areas than ISO achieved. The AKARI maps show many interesting structures and regions related to star formation activity in the Galaxy, tracing the physical processes that trigger high and low mass star formation, and their distribution along the Galactic Plane.

Cygnus X is one of the most complex regions of the Galactic plane fit in the Gould Belt. Its complexity is due to the fact that Cygnus is in the line of sight towards the local spiral arm and so that an enormous quantity of molecular complexes and star forming regions can be observed in it's direction. IRAS satellite confirmed that there is an important star formation activity in the region showing thousands of infrared sources some of them with cold spectra at far infrared wavelengths indicating that they are probably protostellar objects recently formed surrounded by molecular clouds (Dobashi et al., 1994). IRAS also revealed a big population of young stellar objects (YSO) some of which show a complex distribution of high velocity material and outflows which are characteristic of the earliest phase of stellar evolution (Odenwald & Schwartz, 1993). The presence of protostellar objects, YSOs, and outflows suggests that star formation processes are taking place in the molecular clouds of Cygnus.

2. The AKARI diffuse maps calibration

The AKARI diffuse maps show a systematic positional shift compared with data produced by other instruments and also when FIS data observed at two different period are compared. In addition, both the flux calibration and colour corrections must be done separately for diffuse emission maps.

2.1. Positional error

The data used in this section are from AKARI All-Sky Survey observations of the Large Magellanic Cloud, during a two week period in October and November 2006 and two weeks between April and May 2007. Position errors were determined by comparing the locations of several point sources on the LMC maps from both AKARI and from Spitzer data. A systematic position offset was found in the scan direction between AKARI and Spitzer, as well as between the maps performed at different dates. Once the images were shift corrected, the accuracy of the position was verified on the diffuse maps by correlating both the AKARI WS and Spitzer 70 μm maps. The images were shifted one respect the other pixel by pixel and for each new position a new correlation factor was determined. So the correlation array was obtained and the shift value was the difference on the position beween the central position of the array and the position corresponding to the larger value of the correlation factor. Figure 1 shows the correlation between Spitzer and AKARI before and after the shift correction.

2.2. Flux calibration

We used data from the ISO LWS instrument in the parallel mode to calculate the colour correction and the conversion factors.

2.2.1. Colour correction factors

The ISO LWS observed ∼1% of the sky with ten detectors acting as a narrow-band photometer operating at 10 fixed wavelengths between 46 and 180 μm. For each pixel there is a SED that can be fitted by a modified black body curve to estimate the temperature, spectral index

Proceedings of the *"SPICA Joint European Japanese Workshop"*, 6–8 July 2009, Oxford, United Kingdom
(Edited by A. M. Heras, B. M. Swinyard, K. G. Isaak, & J. R. Goicoechea)

Article available at http://spica.edpsciences.org or http://dx.doi.org/10.1051/spica/200903006

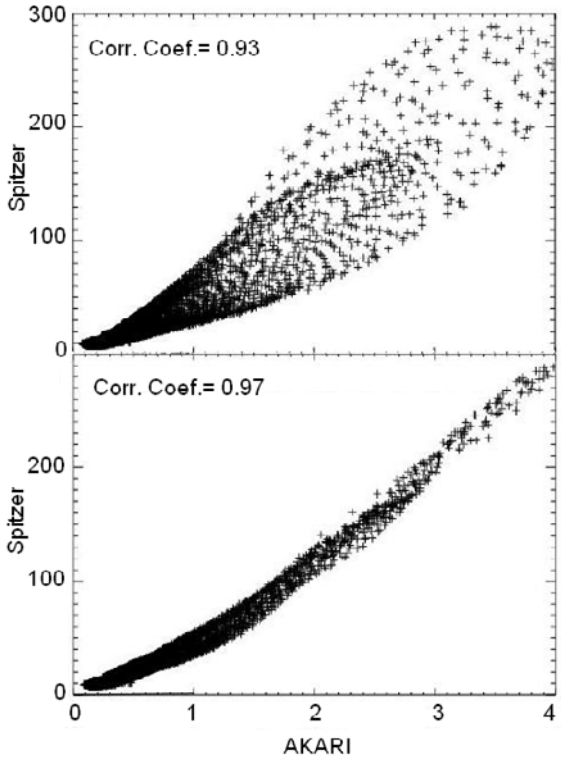

Figure 1. Correlations between Spitzer 70 μm and AKARI WS, before (top) and after (bottom) the shift correction.

and optical depth. Accordingly, the temperature, emissivity and optical depth maps were carried out for various small regions along the galactic plane and colour correction factors (K) were calculated for a black body spectral energy distribution using the temperature and emissivity maps:

$$K = \frac{\int_\nu SED_{spec}\, d\nu}{\int_\nu flat_{spec}\, d\nu} \tag{1}$$

where SED_{spec} is the spectrum bandwith given as:

$$SED_{spec} = RSRF \cdot \frac{\frac{2h\nu^3}{c^2} \cdot \frac{1}{e^{\frac{h\nu}{KT}}-1} \cdot \nu^\beta}{\frac{2h\nu_c^3}{c^2} \cdot \frac{1}{e^{\frac{h\nu_c}{KT}}-1} \cdot \nu_c^\beta} \tag{2}$$

and $flat_{spec}$ is the flat spectrum bandwith:

$$flat_{spec} = RSRF \cdot \frac{\nu_c}{\nu} \tag{3}$$

where $RSRF$ is the Relative Spectral Responsivity Function that was calculated for a flat spectrum ($\nu\ F_\nu = cte$) and ν_c is the frequency at the central wavelength.

2.2.2. Conversion factors

We reproduced ISO intensity maps at 65, 90, 140 and 160 μm using temperature, spectral index and the reference optical depth maps, so the conversion factors were determined as the ratio of ISO Flux (MJy/sr) between AKARI Flux (counts). The colour correction and the conversion factors are given on table 1. The AKARI data already position and colour corrected and turned into MJy/sr using the conversion factors from table 1, show a very good correlation with ISO parallel mode data. Figure 2 show this correlation at 65 and 90 μm.

Table 1. Colour Correction Factors (K) and Conversion Factors (CF).

	K	CF[MJy/sr/counts]
N60	1.06617±0.004	391±6
Wide-S	0.877±0.003	77±2
Wide-L	0.926±0.001	23±1
N160	0.981±0.001	16±1

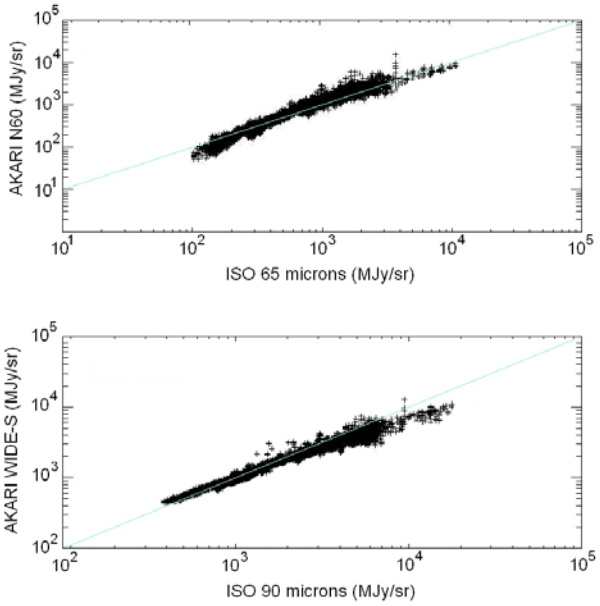

Figure 2. Correlations between the ISO parallel mode data and AKARI data, position and colour corrected, in MJy/sr.

3. An Overview of the AKARI diffuse maps

The AKARI FIS diffuse maps present an opportunity to study distribution and properties of dust, structure and distribution of the star forming regions along the Galactic plane, and the mechanisms that trigger massive-star formation, with better spatial resolution than IRAS achieved. In this section several regions from the AKARI diffuse Galactic plane at 90 μm are compared with IRAS 100 μm.

Figure 3 shows DR15 and G79.29+0.46 in Cygnus star forming region, observed by IRAS at 100 μm and AKARI

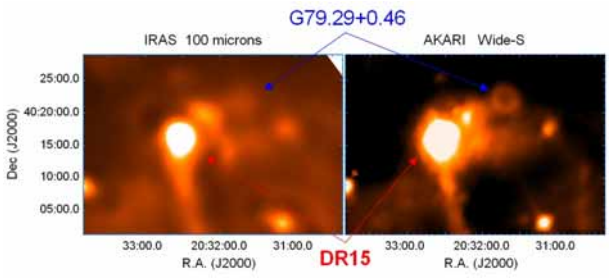

Figure 3. DR15 HII region and G79.29+0.46, a ring like-radio source in the Cygnus X star forming region.

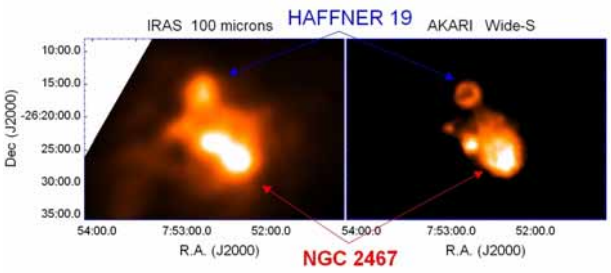

Figure 4. Haffner 19. his is an OB star cluster surrounded by a dusty sphere in the Puppis region.

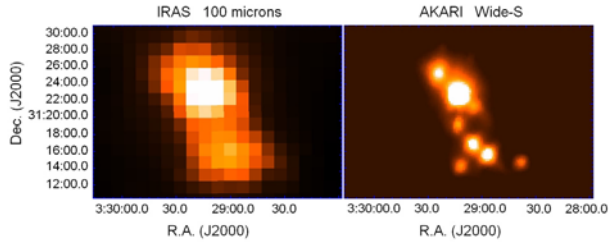

Figure 5. NGC1333 reflection nebula in Perseus.

FIS at 90 μm. DR15 consists of a number of individual HII regions excited by a cluster of young OB stars (Israël, 1977; Colley, 1980). G79.29+0.46 is a ring like radio source that was observed for the first time with the DRAO telescope. It has a faint blue star at its centre that is the responsible for the shell (Waters et al., 1996). Figure 4 reveals NGC2467 HII region, also known as Sharpless 311, at a distance ∼4-5 pc (Pismis & Moreno, 1976), and Haffner 19 HII region.

The IRAS images were taken from the IRS Galaxy Atlas with a high resolution ($\sim 1'$). Both, Haffner 19 on Puppis and the radio source G79.29+0.46 in Cygnus, are detected on the AKARI 90 μm images while they are imperceptible in the IRAS maps at 100 μm, probably because at this wavelength the galactic background is very strong, although IRAS did resolve these features at 24 and 60μm (Waters et al., 1996).

Figure 5 coveres NGC1333 reflexion nebula that is the most active region of star formation in the Perseus molecular cloud. IRAS image at 100 μm with a resolution of $\sim 4'$ was taken from the Skyview, while the AKARI image at 90 μm with a resolution of $\sim$ 40″ is able to resolve the two clumps observed on the IRAS map in a structure of several disconnected clumps.

4. Cygnus X star forming region

Figure 6 is a composite image of Cygnus X at three AKARI FIS bands: 65 μm, 90 μm and 140 μm. The image is centred at: l = 79.76° and b =0.78° with an area of 61.3 degrees. The map looks a bit striped in the scan direction. This stripes are due to changes in the responsivity of the detectors from one scan to the other.

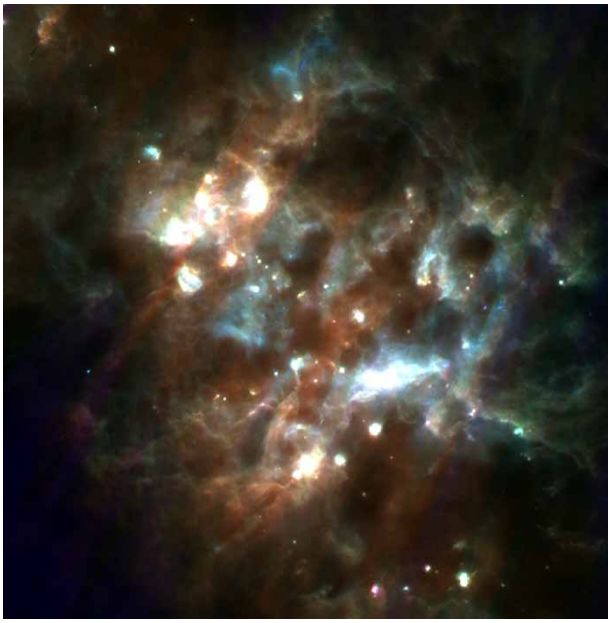

Figure 6. composite image of Cygnus X at three AKARI FIS bands: 65 μm (blue), 90 μm (green) and 140 μm (red).

4.1. The temperature and density maps

We calculated the temperature and the density maps from this region by fitting the four AKARI FIS bands: 65 μm, 90 μm, 140 μm and 160 μm with a modified black body curve (Figure 7). The temperature values of the main regions across Cygnus X are distributed in a range of T∼ 20-35 K. The temperature values obtained are lower than those values determined by Odenwald & Schwartz (1993) who obtained values of T∼ 38-42 K. The hottest areas in the temperature map are distributed tracing the OB asociations: OB9, OB8 and OB2, as well as the area around the HII regions DR22 and DR23, and DR16. A very warm area can be observed at the HII region DR15, with temperatures T∼40 K. There are some very cold objects with temperatures T<10 K. Some of this regions are close to DR21 and W75, spread through a circle centered at $\alpha_{(J2000)}$= 20:37:11, $\delta_{(J2000)}$= +42:26:04. This circle is

one of the most conspicuous feature in the density map, showing very high density values ($N_{H2} > 10^{22}\ cm^{-2}$). This feature also appeared in the density map obtained by Odenwald & Schwartz (1993) and is very good traced by AKARI FIS at 160 μm.

The density map shows very typical values for molecular clouds of $N_H \sim 10^{21}$ cm^{-2}. The West side of the map shows larger densities, $\sim 5 \times 10^{21}$ cm^{-2}, than the East of the map.

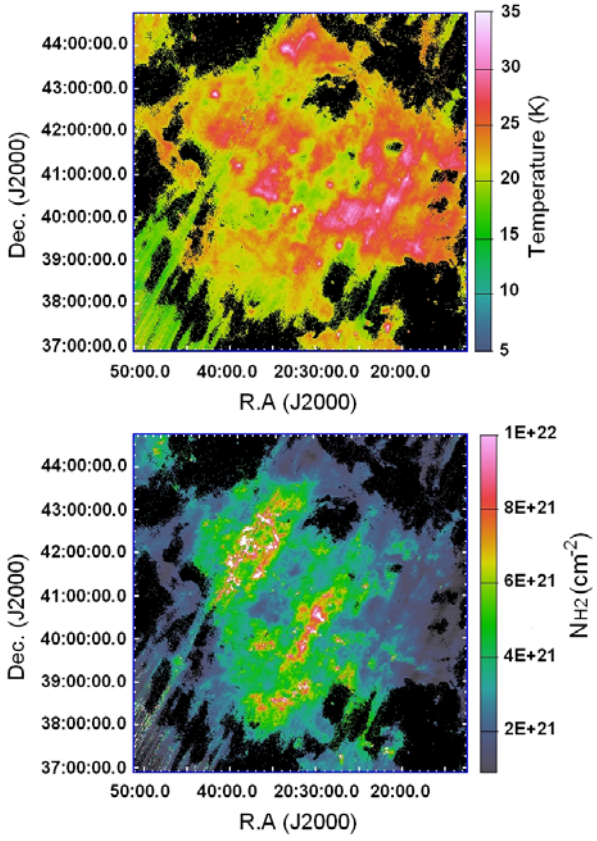

Figure 7. Temperature map (top) and density N_{H2} map (bottom) from Cygnus X region.

4.2. The luminosity function

A matched filter point source extraction routine for clumpy backgrounds was used in order to remove the background of the image. *SExtractor* was used in order to extract all the sources from Cygnus X using a 3σ threshold, once the backgroun was removed. The number of sources extracted by *SExtractor* with an intensity larger than the WS detection limit (0.21 Jy, [5σ/scan]) was 5573. From all these sources, only 800 have fluxes larger than the detection limit for each of the four AKARI bands:

(NS,WS,WL,NL)=(0.94,0.21,1.18,2.5)[Jy, 5σ/scan]

Figure 8 shows the luminosity function in Cygnus X for a distance of 1.7 Kpc (Schneider et al. (2006)), given as:

$$\frac{dN}{dL} = 44,736(\frac{L}{L_\odot})^{-1.048} \quad (4)$$

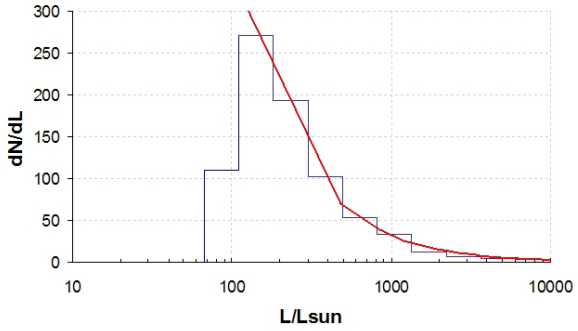

Figure 8. Luminosity function.

The luminosity function shows a maximum number of sources with luminosities in the range 100-200 $L_\odot$. Sources with luminosities $< 60\ L_\odot$ are missing due to the high detection limit of the Wide-L band.

5. Summary

AKARI, with a 0.7 m aperture, completed the All-sky survey covering about 94% of the entire sky with better spatial resolution and wider wavelength coverage than IRAS in the wavelength range from 65 to 180 μm.

SPICA is a cooled infrared observatory whose 3.5 m aperture will provide sensitive data with wider far infrared spectral coverage than AKARI. Its sensitivity will be four orders of magnitude better than AKARI FIS, allowing studies of: galaxies and stars formation; evolution of planetary systems; KBOs, minor planets, comets and other objects in our solar systems, as well as the detection of extrasolar planets due to its high sensitivity.

Acknowledgements

We thank to all the AKARI FIS All-sky survey team.

References

Colley, D. 1980, MNRAS, 192, 377-388
Dobashi, K., Bernard, J.P., Yonekura, Y., Fukui, Y. 1994, ApJS, 95, 419
Israël, F. P. 1977, A&A, 60, 233
Odenwald, S. F., & Schwartz, P. R. 1993, ApJ, 405, 706
Pismis, P., & Moreno, M. A. 1976, RMxAA,1,373
Schneider, N., Bontemps, S., Simon, R., Jacob, H., Motte, F., Miller, M., Kramer, C., Stutzki, J. 2006, A&A, 458, 855
Waters, L. B. F. M., Izumiura, H., Zaal, P. A., Geballe, T. R., Kester, D. J. M., Tj. R. Bontokoe. 1996, A&A, 313, 866